RADAR Imaging – A Mathematical Perspective

P. ELBAU (UNIVERSITY OF VIENNA) AND O. SCHERZER (UNIVERSITY OF VIENNA AND RICAM, AUSTRIAN ACADEMY OF SCIENCES, LINZ)

In this paper we explain with simple geometric arguments the appearance of diffraction hyperbolas in RADAR images. Moreover, we outline an inversion formula from integral geometry, which is derived using only elementary properties of the Fourier transform, to reconstruct the refractive index of a medium from RADAR data. The theoretical results of this paper are supported by real data from an industrial project.

1. Introduction

In this paper we derive some mathematical formulations of RADAR imaging. The objective is to explain by elementary geometric arguments features which are visible in RADAR images. In fact, RADAR images consist of partially overlapping hyperbolas, see Figure 2. Elementary geometrical reasoning can be used to localize isolated objects. The quantitative reconstruction process, on the other hand, that is, the reconstruction of quantitative properties of the reflecting object, turns out to be a classical problem of integral geometry. It can be formulated as a problem of reconstruction of a function from averages over spherical means (see for instance Helgason (2011); Gardner (2006); Agranovsky et al. (2007), to name but a few, and see also the references therein).

This paper is organized as follows: In Section 2 we explain the basic working principle of a RADAR device. Section 3 explains how to locate a single object via trilateration. Section 4 explains the appearance of hyperbolas in RADAR images. Section 5 reports about a practical project of localising avalanche victims using RADAR images. Section 6 discusses the reconstruction of quantitative information using methods from integral geometry.

2. Working principle of a RADAR system

A RADAR system (an acronym for "Radio Detection And Ranging") is designed to detect distant objects by emitting a short electromagnetic pulse in the radio frequency spectrum, that is, with a wavelength larger than infrared light, which is less reflected and distorted by the atmosphere than usual light, and thus allows also to inspect objects which are hidden behind clouds, for example.

This pulse then propagates as a spherical wave with the speed of light. When it hits an object, a part of this wave is reflected. This reflection again propagates as a spherical wave with center at this object and will thus also arrive back at the position of the RADAR device, which records the reflected waves.

In particular, by measuring the time t between the emission of the pulse and the arrival of the reflected electromagnetic wave, we can calculate from the known wave speed, the speed of light c, the distance r of the object: $r = \frac{t}{2c}$. However, in this setup, we do lack the information to uniquely locate the object of interest.

3. Object Localisation with Trilateration

If there is only one object reflecting the emitted radio wave, we can find its position by multiple measurements via trilateration: Assume we make a RADAR measurement from three different positions $x_0, x_1, x_2 \in \mathbb{R}^3$. At each position we obtain the distances $r_i = |x_i - x|$, $i = 0,1,2$, between the unknown position $x \in \mathbb{R}^3$ of the object and the known positions $x_i \in \mathbb{R}^3$ of our RADAR device. Then, the point x lies on the intersection of the three spheres $\partial B_{r_i}(x_i)$, which consists of only two points if the positions x_i, $i = 0,1,2$, are not colinear (that is, if they do not lie on a single line).

Proposition 3.1 *Let $x_i \in \mathbb{R}^3$, $i = 0,1,2$, be three given points which are not colinear. Then, a point $x \in \mathbb{R}^3$ with*

$$|x - x_i| = r_i, \quad i=0,1,2,$$

for some given distances $r_i \geq 0$, $= 0,1,2$, has an explicit coordinate representation of the form

$$x = x_0 + \sum_{i=1}^{3} \alpha_i e_i \tag{1}$$

with respect to the (non-orthogonal) basis $\{e_1, e_2, e_3\}$ given by

$$e_1 = \frac{x_1 - x_0}{|x_1 - x_0|}, \quad e_2 = \frac{x_2 - x_0}{|x_2 - x_0|}, \quad e_3 = \frac{e_1 \times e_2}{|e_1 \times e_2|},$$

where

$$\alpha_1 = \frac{\beta_1 - \beta_2 \langle e_1, e_2 \rangle}{1 - \langle e_1, e_2 \rangle^2}, \qquad \beta_1 = \frac{r_0^2 - r_1^2 + |x_1 - x_0|^2}{2|x_1 - x_0|}, \tag{2}$$

$$\alpha_2 = \frac{\beta_2 - \beta_1 \langle e_1, e_2 \rangle}{1 - \langle e_1, e_2 \rangle^2}, \qquad \beta_2 = \frac{r_0^2 - r_2^2 + |x_2 - x_0|^2}{2|x_2 - x_0|}, \tag{3}$$

$$\alpha_3^2 = r_0^2 - |\alpha_1 e_1 + \alpha_2 e_2|^2. \tag{4}$$

Proof: We first observe that for $i = 1,2$

$$\langle x - x_0, x_i - x_0 \rangle = r_0^2 - \langle x - x_0, x - x_i \rangle = r_0^2 + \frac{1}{2}(|x_i - x_0|^2 - r_0^2 - r_i^2) = |x_i - x_0|\beta_i,$$

where $\langle \cdot, \cdot \rangle$ denotes the standard inner product on $\mathbb{R}^3$: $\langle k, y \rangle = k_1 y_1 + k_2 y_2 + k_3 y_3$. Thus, we get for the decomposition (1) that

$$\alpha_1 + \alpha_2 \langle e_1, e_2 \rangle = \langle x - x_0, e_1 \rangle = \beta_1,$$
$$\alpha_1 \langle e_1, e_2 \rangle + \alpha_2 = \langle x - x_0, e_2 \rangle = \beta_2.$$

Solving this linear equation system, we arrive at the formulas (2) and (3) for α_1 and α_2. Finally, the last coefficient α_3 is determined by taking the norm of $x - x_0$:

$$r_0^2 = |x - x_0|^2 = |\alpha_1 e_1 + \alpha_2 e_2|^2 + \alpha_3^2,$$

which gives (4).

Usually, only one of the two choices for α_3 in the representation (1), explicitly given by formula (4), is physically meaningful. But we could still perform a fourth measurement from a point $x_3 \in \mathbb{R}^3$ outside the plane through the three points x_0, x_1, and x_2 to decide which of the two coefficients α_3 is correct.

4. Identifying Different Objects

However, in practice, there is not just one reflecting object, but instead every object produces some signal of different strength so that we get simply a varying signal intensity and it is not trivial, how to identify signals and corresponding objects. So, we first have to find which points in the signals of the three different measurements correspond to the same object, before we can calculate the position of this object.

To do so, let us not only consider three different measurement positions, but vary our position continuously. How does the signal of an object change during this motion?

Proposition 4.1 *Let $\gamma : \mathbb{R} \to \mathbb{R}^3$ be the parametrisation of a straight line:*

$$\gamma(\tau) = x_0 + v\tau$$

for some initial position $x_0 \in \mathbb{R}^3$ and a velocity $v \in \mathbb{R}^3 \setminus \{0\}$.

Then, the distance

$$r(\tau) = |x - \gamma(\tau)|$$

fulfils the equation

$$\frac{r^2(\tau)}{a^2} - \frac{(\tau - \tau_0)^2}{b^2} = 1 \tag{5}$$

of a hyperbola with center in $(0, \tau_0)$ and half axes

$$a = \sqrt{|x - x_0|^2 - |v|^2\tau_0^2} \quad \text{and} \quad b = \frac{a}{|v|},$$

where

$$\tau_0 = \frac{\langle x - x_0, v \rangle}{|v|^2}$$

is the time at which the distance between x and the curve γ is minimal, see Figure 1.

Proof: We have that

$$r^2(\tau) = |x - x_0 - v\tau|^2 = |x - x_0|^2 - 2\langle x - x_0, v \rangle \tau + |v|^2\tau^2.$$

Completing the square gives us

$$r^2(\tau) = |v|^2 \left(\tau - \frac{\langle x - x_0, v \rangle}{|v|^2} \right)^2 + |x - x_0|^2 - \frac{\langle x - x_0, v \rangle^2}{|v|^2} = |v|^2(\tau - \tau_0)^2 + a^2,$$

which can be rewritten in the standard form (5).

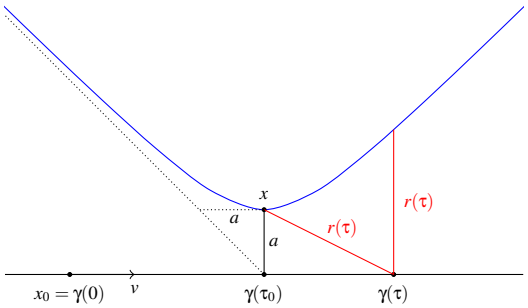

Fig. 1: Plotting the distances $r(\tau)$ between the point x and the points $\gamma(\tau) = x_0 + v\tau$, $\tau \in \mathbb{R}$, for some vector $v \in \mathbb{R}^3 \setminus \{0\}$ as a function of the distance $|\gamma(\tau) - x_0| = v\tau$ gives the hyperbola $r^2(\tau) - (v\tau - v\tau_0)^2 = a^2$, where τ_0 is chosen such that $\gamma(\tau_0)$ is the point on the curve γ with minimal distance to x.

Thus, if we plot the intensity of the measured signal as a function of observation time t and of the position $\gamma(\tau)$ of the RADAR device, we should see peaks in the intensity along hyperbolas corresponding to strongly reflecting objects.

If we then do two of these measurement along two different intersecting straight lines, say γ_1 and γ_2 with $\gamma_1(0) = \gamma_2(0)$, we can identify in the measurements for three different positions, say $x_0 = \gamma_1(0)$,

$x_1 = \gamma_1(1)$ and $x_2 = \gamma_2(1)$, the signal corresponding to some object, and therefore reconstruct its position via trilateration as described in Section 3.

Looking at some real data, see Figure 2, we see the predicted hyperbolas. That we only see a small part of the hyperbolas is mainly due to the fact that in practice the RADAR waves are focused in some direction and thus only reach the object if it is in focusing direction. Additionally, the waves lose intensity as they travel through the material which weakens the signal from more distant objects and therefore the objects are best seen when they are closest, that is around the vertex of the hyperbola.

5. A Practical Application: Locations of Victims in Avalanches

The technique of localising objects which visually may be hidden, but are reachable with radio frequencies, can be for example used to detect victims and bodies which were trapped by an avalanche under the snow. In a project of the Comet-K1-Zentrum "alpS - Centre for Climate Change Adaptation" we have been involved in trials for locating avalanche victims with a mobile RADAR device which is mounted on a helicopter which flies with relatively constant speed along a straight line γ over the avalanche area where victims are suspected. At each position $\gamma(\tau)$, determined by the flying time τ, the RADAR device sends out a radio wave towards the ground and records the reflected waves as a function of the time t after the emission, see Figure 2 for a picture of the helicopter and a sample of recorded data. (We hereby neglect that the helicopter also moves during one of these measurements, since the travel time of such a radio wave, assuming a distance to the ground is at most of the order of a few kilometres, is only of the order of microseconds.)

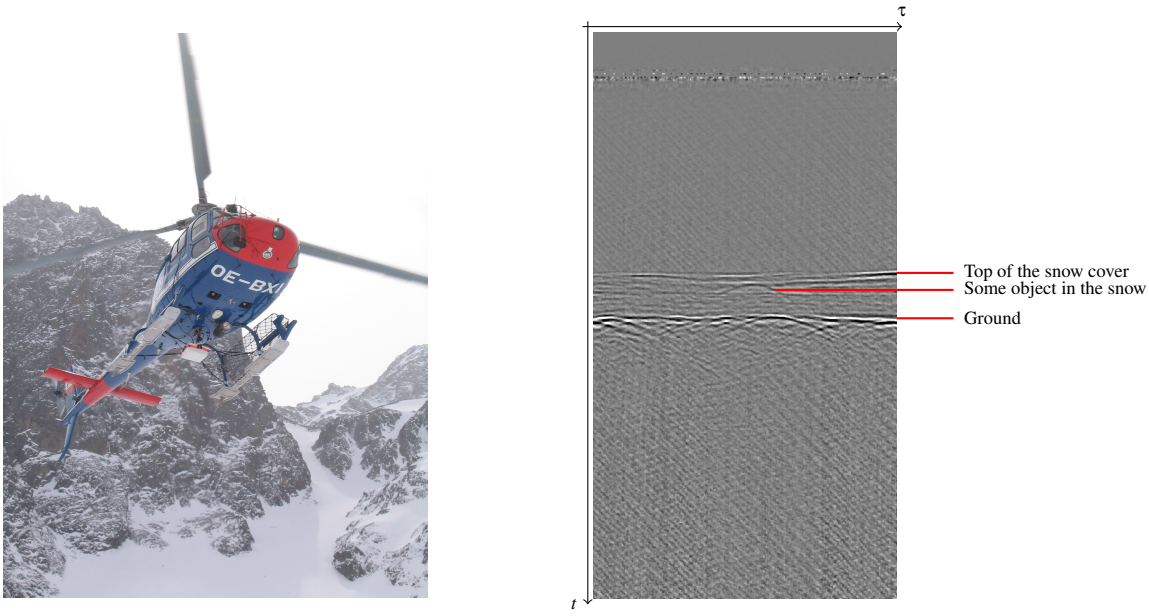

Fig. 2: An image of the helicopter which was equipped with the mobile RADAR device, and the recorded intensity of the reflected RADAR signal as a function of time t after the initial pulse at every position $\gamma(\tau)$ of the helicopter during its search for a simulated avalanche victim.

6. Quantitative Reconstruction

Looking at the real measurement data in Figure 2, we see that the assumption of having only some distinct reflecting objects is not really realistic. Instead, we rather want to assume that at every point some part of the incoming wave is reflected and what we see as signal is simply the different amount of reflection. So, let us introduce the reflection coefficient $n(y) \in [0,1]$ specifying the percentage of the wave which is reflected at a point $y \in \mathbb{R}^3$.

Then, after the time t (measured from the time where the radio pulse is emitted), we detect all the reflected waves which originate from points which are at distance $r = \frac{t}{2c}$. Therefore, the RADAR measurement at a position $x \in \mathbb{R}^3$ provides us (after correcting with the intensity of the initial wave and the intensity loss of the reflecting wave) with the integral of the values of the reflection coefficient over the sphere $\partial B_r(x)$ with radius r and center x:

$$m(r,x) = \int_{\partial B_r(x)} n(y)\,\mathrm{d}s(y).$$

How can we extract now from this information the function $n : \mathbb{R}^3 \to \mathbb{R}$? Clearly, measurements at one point $x \in \mathbb{R}^3$ are not enough, but if we make measurements at every position $x \in E$ in a plane $E \subset \mathbb{R}^3$, then it turns out that we can explicitly reconstruct n. To show this, we will make use of the Fourier transform. We give here the inversion formula for the Fourier transform without proof, see for example (Feeman, 2010, Chapter 5) for more details on the Fourier transform.

Theorem 6.1 *For every smooth function $f : \mathbb{R} \to \mathbb{R}$ with compact support, there exists a unique smooth function $\hat{f} : \mathbb{R} \to \mathbb{R}$, the Fourier transform of f, such that for every $x \in \mathbb{R}$ the identity*

$$f(x) = \frac{1}{\sqrt{2\pi}} \int_{-\infty}^{\infty} \hat{f}(k) \mathrm{e}^{\mathrm{i}kx}\,\mathrm{d}k$$

holds. This function $\hat{f}$ is explicitly given by

$$\hat{f}(k) = \frac{1}{\sqrt{2\pi}} \int_{-\infty}^{\infty} f(y) \mathrm{e}^{-\mathrm{i}ky}\,\mathrm{d}y.$$

We may also write this result in terms of trigonometric functions.

Corollary 6.2 *For every odd, smooth function $f : \mathbb{R} \to \mathbb{R}$ with compact support, there exists a unique smooth function $\tilde{f} : \mathbb{R} \to \mathbb{R}$ such that for every $x \in \mathbb{R}$ the identity*

$$f(x) = \sqrt{\frac{2}{\pi}} \int_0^{\infty} \tilde{f}(k) \sin(kx)\,\mathrm{d}k \tag{6}$$

holds. The function $\tilde{f}$ is explicitly given by

$$\tilde{f}(k) = \sqrt{\frac{2}{\pi}} \int_0^{\infty} f(y) \sin(ky)\,\mathrm{d}y.$$

Proof: Since f is odd, the Fourier transform $\hat{f}$ of f is of the form

$$\hat{f}(k) = \frac{1}{\sqrt{2\pi}} \int_{-\infty}^{\infty} f(y) \mathrm{e}^{-\mathrm{i}ky}\,\mathrm{d}y = \frac{1}{\sqrt{2\pi}} \int_{-\infty}^{\infty} f(y)(\cos(ky) - \mathrm{i}\sin(ky))\,\mathrm{d}y = -\mathrm{i}\sqrt{\frac{2}{\pi}} \int_0^{\infty} f(y)\sin(ky)\,\mathrm{d}y.$$

Thus, $\hat{f}(k) = -\mathrm{i}\tilde{f}(k)$ is purely imaginary and we find that

$$f(x) = \mathfrak{Re}(f(x)) = \frac{1}{\sqrt{2\pi}} \int_{-\infty}^{\infty} \mathfrak{Re}(\hat{f}(k)\mathrm{e}^{\mathrm{i}kx})\,\mathrm{d}k = \frac{1}{\sqrt{2\pi}} \int_{-\infty}^{\infty} \tilde{f}(k)\sin(kx)\,\mathrm{d}k.$$

Since $\tilde{f}$ is clearly odd, we get (6).

Finally, let us come to the reconstruction of the reflection coefficient from the measurements.

Proposition 6.3 *Let $n : \mathbb{R}^3 \to \mathbb{R}$ be a smooth function with compact support and assume that we know the values*

$$m(r,x) = \int_{\partial B_r(x)} n(y)\,\mathrm{d}s(y) = \int_{\partial B_r(0)} n(x+y)\,\mathrm{d}s(y) \tag{7}$$

for all $r > 0$ and every $x \in \mathbb{R}^3$ with $x_3 = 0$. Then, the function n fulfils the relation

$$n(y_1,y_2,y_3) + n(y_1,y_2,-y_3) = \frac{1}{4\pi^3} \int_{\mathbb{R}^3} \int_0^\infty \hat{m}(r,k_1,k_2,0) \frac{k_3 \sin(|k|r)}{r} \mathrm{e}^{\mathrm{i}\langle k,y\rangle} \,\mathrm{d}r\,\mathrm{d}k, \quad y \in \mathbb{R}^3, \tag{8}$$

where $\hat{m}$ is the Fourier transform of m with respect to x_1 and x_2:

$$\hat{m}(r,k_1,k_2,x_3) = \frac{1}{2\pi} \int_{-\infty}^\infty \int_{-\infty}^\infty m(r,x_1,x_2,x_3) \mathrm{e}^{-\mathrm{i}(k_1x_1+k_2x_2)} \,\mathrm{d}x_1\,\mathrm{d}x_2, \quad r > 0,\ k_1,k_2,x_3 \in \mathbb{R}. \tag{9}$$

Proof: Writing the function n in terms of its Fourier transform with respect to all three components, we find according to Theorem 6.1 that

$$m(r,x) = \frac{1}{(2\pi)^{\frac{3}{2}}} \int_{\mathbb{R}^3} \int_{\partial B_r(0)} \hat{n}(k) \mathrm{e}^{\mathrm{i}\langle k,x+y\rangle} \,\mathrm{d}s(y)\,\mathrm{d}k,$$

where

$$\hat{n}(k) = \frac{1}{(2\pi)^{\frac{3}{2}}} \int_{\mathbb{R}^3} n(y) \mathrm{e}^{-\mathrm{i}\langle k,y\rangle} \,\mathrm{d}y.$$

To calculate the inner integral, we consider a rotation $R \in \mathrm{SO}(3)$ which maps the vector k into $|k|(0,0,1)^\mathrm{t}$. In this way, we get for $y = R^\mathrm{t} z$

$$\langle k,y\rangle = \left\langle k, R^\mathrm{t} z\right\rangle = \langle Rk, z\rangle = |k| \left\langle \begin{pmatrix} 0 \\ 0 \\ 1 \end{pmatrix}, z \right\rangle = |k| z_3.$$

Then it follows by using spherical coordinates $z = r(\sin\theta\cos\varphi, \sin\theta\sin\varphi, \cos\theta)^\mathrm{t}$:

$$\begin{aligned} \int_{\partial B_r(0)} \mathrm{e}^{\mathrm{i}\langle k,y\rangle} \,\mathrm{d}s(y) &= \int_{\partial B_r(0)} \mathrm{e}^{\mathrm{i}|k|z_3} \,\mathrm{d}s(z) = \int_0^{2\pi} \int_0^\pi \mathrm{e}^{\mathrm{i}|k|r\cos\theta} r^2 \sin\theta \,\mathrm{d}\theta\,\mathrm{d}\varphi \\ &= -\frac{2\pi r}{\mathrm{i}|k|} \mathrm{e}^{\mathrm{i}|k|r\cos\theta} \Big|_0^\pi = 4\pi r \frac{\sin(|k|r)}{|k|}. \end{aligned}$$

Thus, we get

$$m(r,x) = r\sqrt{\frac{2}{\pi}} \int_{\mathbb{R}^3} \hat{n}(k) \frac{\sin(|k|r)}{|k|} \mathrm{e}^{\mathrm{i}\langle k,x\rangle} \,\mathrm{d}k.$$

If we restrict this now to values $x \in \mathbb{R}^3$ with $x_3 = 0$, then this is seen to be of the form of a Fourier transform with respect to x_1 and x_2, and we find with the notation (9) that

$$\hat{m}(r,k_1,k_2,0) = 2r\sqrt{2\pi} \int_{-\infty}^\infty \hat{n}(k) \frac{\sin(|k|r)}{|k|} \,\mathrm{d}k_3.$$

We split the integral now in one over the positive values and one over the negative values of k_3. In the latter, we then substitute k_3 by $-k_3$ and combine the integrals again. This gives us

$$\hat{m}(r,k_1,k_2,0) = 2r\sqrt{2\pi} \int_0^\infty (\hat{n}(k_1,k_2,k_3) + \hat{n}(k_1,k_2,-k_3)) \frac{\sin(|k|r)}{|k|} \,\mathrm{d}k_3.$$

Next, we substitute k_3 by the variable

$$\kappa = |k|, \quad \text{that is} \quad k_3(\kappa) = \sqrt{\kappa^2 - k_1^2 - k_2^2}.$$

This yields with the volume element $\mathrm{d}k_3(\kappa) = \frac{\kappa}{k_3(\kappa)}\,\mathrm{d}\kappa$:

$$\frac{1}{2\pi r}\hat{m}(r,k_1,k_2,0) = \sqrt{\frac{2}{\pi}}\int_{\sqrt{k_1^2+k_2^2}}^{\infty} \frac{\hat{n}(k_1,k_2,k_3(\kappa)) + \hat{n}(k_1,k_2,-k_3(\kappa))}{k_3(\kappa)} \sin(\kappa r)\,\mathrm{d}\kappa.$$

This is now of the form (6) with

$$\tilde{f}(\kappa) = \begin{cases} \frac{1}{k_3(\kappa)}(\hat{n}(k_1,k_2,k_3(\kappa)) + \hat{n}(k_1,k_2,-k_3(\kappa))) & \text{if } \kappa \geq \sqrt{k_1^2+k_2^2}, \\ 0 & \text{if } \kappa < \sqrt{k_1^2+k_2^2}. \end{cases}$$

Therefore, we find that

$$\sqrt{\frac{2}{\pi}}\int_0^{\infty} \frac{\hat{m}(r,k_1,k_2,0)}{2\pi r} \sin(\kappa r)\,\mathrm{d}r = \frac{\hat{n}(k_1,k_2,k_3(\kappa)) + \hat{n}(k_1,k_2,-k_3(\kappa))}{k_3(\kappa)}$$

for every $\kappa \geq \sqrt{k_1^2+k_2^2}$.

Switching back to the variable k_3 instead of κ, multiplying with k_3, and doing an inverse Fourier transform with respect to k_1, k_2, and k_3, we get the formula (8).

So, by calculating the right hand side of (8), we obtain the symmetric combination of the reflection coefficient n. To get the reflection coefficient itself, we could only register signals originating from points $y \in \mathbb{R}^3$ with $y_3 > 0$. This would correspond to setting $n(y) = 0$ whenever $y_3 \leq 0$, so that we can drop the second term on the left hand side of (8) and obtain the desired reconstruction formula for n.

Remark 6.4 *The reconstruction formula* (8) *can actually be used to determine the reflection coefficient n. However, the practical realization requires a dense set of measurement on the whole two-dimensional Euclidean domain. For the avalanche victims detection problem we require the helicopter to fly in a path which covers at least the area of the locations of victims and a sufficiently dense flight path. Missing measurement regions and not a sufficiently dense data recording results into artefacts, which can be explained with micro-local analysis, see Frikel and Quinto (2015). A numerical inversion of the back-projection formula for RADAR images has been investigated in Grasmair et al. (2015).*

Conclusion

In this paper we have explained certain features in RADAR images. We have shown that the inversion process for the refractive index is in fact a problem of integral geometry. The theoretical result of this paper are complemented by some report about an industrial project for locating avalanche victims.

Acknowledgement

This work is supported by the Austrian Science Fund (FWF), Project P26687-N25 (Interdisciplinary Coupled Physics Imaging). The avalanche project outlined was performed at the Comet-K1-Zentrum “alpS - Centre for Climate Change Adaptation”.

Literatur

M. L. Agranovsky, K. Kuchment, and E. T. Quinto. Range descriptions for the spherical mean Radon transform. *J. Funct. Anal.*, 248(2):344–386, 2007.

T. G. Feeman. *The Mathematics of Medical Imaging*. Springer Undergraduate Texts in Mathematics and Technology. Springer, New York, 2010. doi: 10.1007/978-0-387-92712-1.

J Frikel and E. T. Quinto. Artifacts in incomplete data tomography with applications to photoacoustic tomography and sonar. *SIAM J. Appl. Math.*, 75(2):703–725, 2015. doi: 10.1137/140977709.

R. J. Gardner. *Geometric tomography*. Number 58 in Encyclopedia of Mathematics and its Applications. Cambridge University Press, Cambridge, 2 edition, 2006. ISBN 978-0-521-68493-4; 0-521-68493-5.

M. Grasmair, M. Haltmeier, and O. Scherzer. Sparsity in inverse geophysical problems. In W. Freeden, M. Z. Nashed, and T. Sonar, editors, *Handbook of Geomathematics*. Springer Berlin Heidelberg, 2015. ISBN 978-3-642-27793-1. doi: 10.1007/978-3-642-27793-1_25-2.

S. Helgason. *Integral Geometry and Radon Transform*. Springer, New York, NY, 2011. ISBN 978-1-4419-6054-2.